Monthly Notices
of the
ROYAL ASTRONOMICAL SOCIETY

MNRAS **451,** 2922–2932 (2015) doi:10.1093/mnras/stv1157

The galactic branches as a possible evidence for transient spiral arms

Angeles Pérez-Villegas,[1,2⋆] Gilberto C. Gómez[1⋆] and Bárbara Pichardo[3⋆]

[1]*Centro de Radioastronomía y Astrofísica, Universidad Nacional Autónoma de México, Apdo. postal 3-72, Morelia Mich. 58089, Mexico*
[2]*Max-Planck-Institüt für Extraterrestrische Physik, Gießenbachstraße, D-85741 Garching, Germany*
[3]*Instituto de Astronomía, Universidad Nacional Autónoma de México, Apdo. postal 70-264 Ciudad Universitaria, D.F. 04510, Mexico*

Accepted 2015 May 18. Received 2015 March 27; in original form 2014 December 16

ABSTRACT

With the use of a background Milky Way-like potential model, we performed stellar orbital and magnetohydrodynamic simulations. As a first experiment, we studied the gaseous response to a bisymmetric spiral arm potential: the widely employed cosine potential model and a self-gravitating three-dimensional density distribution based model called PERLAS. Important differences are noticeable in these simulations, while the simplified cosine potential produces two spiral arms for all cases, the more realistic density-based model produces a response of four spiral arms on the gaseous disc, except for weak arms – i.e. close to the linear regime – where a two-armed structure is formed. In order to compare the stellar and gas response to the spiral arms, we have also included a detailed periodic orbit study and explored different structural parameters within observational uncertainties. The four-armed response has been explained as the result of ultraharmonic resonances, or as shocks with the massive bisymmetric spiral structure, among other. From the results of this work, and comparing the stellar and gaseous responses, we tracked down an alternative explanation to the formation of branches, based only on the orbital response to a self-gravitating spiral arms model. The presence of features such as branches, might be an indication of transiency of the arms.

Key words: MHD – Galaxy: disc – Galaxy: kinematics and dynamics – Galaxy: structure – galaxies: spiral – galaxies: structure.

1 INTRODUCTION

Spiral arms are one of the most striking, beautiful and scientifically challenging structures of disc galaxies. They have fascinated and intrigued astronomers for centuries. As a rough initial approximation to treat this complex problem, the spiral arms had to be assumed as almost massless and/or with extremely modest pitch angles, in order to obtain a solution as a linear perturbation to the axisymmetric background potential. The proposed solution to the permanence of spiral arms in galaxies was based on the spiral density wave linear theory (Lin & Shu 1964, inspired in the 1960s work of B. Lindblad and P.O. Lindblad). The analytical solution at first order of the theory, known as the tight-winding approximation (TWA), that represents a weak potential model, extremely idealized as a smooth, even negligible perturbation to the background potential, was modelled as a simplified cosine function to represent the spiral arms gravitational potential. Probably followed by this initial attempt of solving the nature of spiral arms, a lot of work has tackled repeatedly the problem of modelling them, as a simplified periodic function that disregards the importance of their dynamical effects. However, spiral arms have proven to be an influential feature on galactic modern models (such as PERLAS and *N*-body models, based on three-dimensional density structures), far beyond of a simple smooth perturbation.

If we compare the spiral arms with the galactic bar, the latter has a mass between 10 and 20 per cent of the disc mass (Matsumoto et al. 1982; Dwek et al. 1995; Zhao 1996; Weiner & Selwood 1999), unlike the spiral arms that have a mass smaller in general than 5 per cent of the disc mass (Pichardo et al. 2003). Consequently, the largest influence on the disc of strongly barred galaxies is, of course, due to the central bar. Therefore one would be tempted to oversimplify the scenario, by assuming that spiral arms are not influential at all on the dynamics of the disc. However, there are determinations that suggest that the majority of spiral galaxies, or at least those with clearly delineated spiral arms, are rather far from being linear (Pichardo et al. 2003; Voglis, Stavropoulos & Kalapotharakos 2006; Antoja et al. 2009, 2010, 2011; Sellwood 2011; Roca-Fàbrega et al. 2013, 2014; Kawata et al. 2014; Sellwood & Carlberg 2014).

Based on all those rigorous studies, spiral arms seem to merit an extra effort to model them beyond a simple perturbing term. This fact is even more significant in the case of the interstellar gas, which is considerably more sensitive to the details of the potential, and in general, responds strongly even if the mass of the spiral arms is only a small fraction of the axisymmetric background (Shu, Milione &

⋆ E-mail: mperez@mpe.mpg.de (AP-V); g.gomez@crya.unam.mx (GCG); barbara@astro.unam.mx (BP)

Roberts 1973; Gómez, Pichardo & Martos 2013; Kim, Kim & Kim 2014).

For almost a century, formal studies of spiral arms have been carried on. Yet, the spiral arms morphology, origin and nature are still poorly understood. With respect to their morphology, there is plentiful theoretical and observational literature on structures related to spiral arms, such as spurs, branches, feathers and beads, and their plausible explanations (Lynds 1970; Weaver 1970; Shu et al. 1973; Sofue 1976; Elmegreen 1980; Balbus 1988; Scoville et al. 2001; Kim & Ostriker 2002; Chakrabarti, Laughlin & Shu 2003; Kim & Ostriker 2006; Shetty & Ostriker 2006; Corder et al. 2008; Dobbs, Burkert & Pringle 2011; Lee & Shu 2012). Regarding spurs and feathering, interesting scenarios to explain these features include plain hydrodynamic simulations, where the Kelvin–Helmholtz instability creates spurs produced by shocks with the spiral arms (Wada & Koda 2004, an extension to self-gravitating three-dimensional models of this work is presented in Kim & Ostriker 2006). Other scenarios include the use of global magnetohydrodynamic (MHD) simulations, adding gas self-gravity and magnetic fields that produce differential compression of gas flowing through the arms resulting in the formation of sheared structures in the interarm regions that resemble spurs and feathers (Kim & Ostriker 2002; Shetty & Ostriker 2006), or through gravitational or magneto-Jeans instabilities (Balbus 1988).

On the other hand, features such as branches are significantly longer than spurs that emerge almost parallel to the main spiral arms but with different pitch angles (usually smaller), and are generally associated with resonances. It is worth to note that, in the literature, the names spurs, feathers and branches are assigned to slightly different structures. In this work, we will adopt the definition given by Feitzinger & Schwerdtfeger (1982) and Chakrabarti et al. (2003), where the 'spurs' and 'feathers' are small structures that arise almost perpendicularly from the main spiral arm, and 'branches' are narrow structures that arise almost parallel to the main spiral arm, with smaller pitch angles and extension longer than spurs (examples of branches can be seen in galaxies like NGC 309, NGC 1637, NGC 2997, NGC 6946, among others). Regarding such structures, theory and gas simulations have already shown a bifurcation of spiral arms produced by ultraharmonic resonances induced by the main spiral arm on the background gas flow (Shu et al. 1973; Artymowicz & Lubow 1992; Patsis et al. 1994; Patsis, Grosbol & Hiotelis 1997; Chakrabarti et al. 2003). In this case, the bifurcation of the arms is expected due to the topology of the stable periodic orbits at the 4/1 resonance. Other interpretations also include the possibility that branches are the response of the gas produced by strong shocks against the main massive spiral arms, i.e. the ones made mainly of older and smaller stars (Barbanis & Woltjer 1967; Fujimoto 1968; Roberts 1969; Shu et al. 1973; Roberts, Huntley & van Albada 1979; Chakrabarti, Laughlin & Shu 2003; Martos et al. 2004; Yañez et al. 2008; Kim & Kim 2014).

Specifically, regarding the Milky Way Galaxy, its general structure has been extensively studied and the latest determinations seem to agree with two grand design symmetric spiral arms, seen on IR and optical, and some other weaker arms, detectable mainly in optical observations (Drimmel 2000; Drimmel & Spergel 2001; Vallée 2002, 2013; Benjamin et al. 2005). The weaker arms (branches) have been explained through hydrodynamic simulations as the response to the two-armed stellar pattern. For example, Englmaier & Gerhard (1999) and Fux (1999) found that the gas response to a barred potential can produce a four-armed spiral structure. Likewise, from hydrodynamic and MHD simulations, the gas responds to an imposed two-armed spiral potential with four spiral arms (Shu et al. 1973; Martos et al. 2004; Gómez et al. 2013). In this context, the gas component shocks at the position of the spiral arms, producing a density enhancement and star formation (Fujimoto 1968; Roberts 1969; Moore et al. 2012; Seo & Kim 2014) that, depending on the relative velocity between the gas and the spiral arm, dwell upstream or downstream or in the spiral arm. In particular, Roberts (1969) showed that the non-linear response of the gas to a stationary stellar spiral arm potential may produce two shocks, which then would be associated with a doubling of the spiral arm number as seen in the gas component. Shu et al. (1973) demonstrated that shocks in galaxies arise necessarily if the spiral arm strength exceeds a certain critical value. Additionally, they found a range of values for the wave frequency that generates an ultraharmonic resonance which can provoke a secondary compression of the interstellar gas. This effect has been related to the origin of the Carina arm in the Milky Way (Shu et al. 1973), for example. However, since branches have been traditionally explained as shocks induced by the spiral arms, it is important to mention other observational work that shows there is little difference (or none at all) in the star formation efficiency (i.e. no shocks) between the spiral arms regions and the rest of the disc (Foyle et al. 2010, 2011; Dobbs et al. 2011; Eden et al. 2013).

Finally, regarding their nature, a problem of great interest is whether spiral arms are a transient or a long-lived feature. On this matter, recent numerical simulations show that spiral arms are transient and recurrent structures (Dobbs & Bonnell 2006; Foyle et al. 2011; Sellwood 2011; Wada, Baba & Saitoh 2011; Pérez-Villegas et al. 2012; Roškar et al. 2012; D'Onghia, Vogelsberger & Hernquist 2013; Pérez-Villegas, Pichardo & Moreno 2013; Kawata et al. 2014; Sellwood & Carlberg 2014). However, in a study by Scarano & Lépine (2013) on a sample of 27 galaxies, the authors concluded that the break found in the radial metallicity distribution near to corotation resonance (CR), implies that the spiral structure is a rather long-lived feature. Other authors, employing different techniques, seem to find observational proofs of long-lasting spiral arms (Donner & Thomasson 1994; Zhang 1998; Martínez-García & González-López lira 2013).

In this work, we explore the gas response to a bisymmetric spiral arm potential. For this purpose, we employed two different models, a cosine potential (generally used in literature) and the three-dimensional, density distribution based potential PERLAS, applied to the particular case of a Milky Way-like galaxy. With this study, we find an alternative explanation to the formation of branches in disc galaxies, and their relation to transient or long-lived spiral arms.

This paper is organized as follows. In Section 2, the galactic potential used to compute the stellar orbits and the MHD initial simulation set-up are described. In Section 3, we present first a comparison between the models of the spiral arms: PERLAS and the cosine potential; second, we present the gas response to spiral arms PERLAS model changing the structural parameters such as the pitch angle and the mass of the spiral arms, and their connection with the presence of galactic branches as a signature of transient spiral arms. Finally, we present a discussion and our conclusions in Section 4.

2 METHODOLOGY AND NUMERICAL IMPLEMENTATION

Motivated by the fact that the gas in galaxies is dynamically colder than the stellar disc, in addition to being collisional, we can expect it to be much more sensitive to details of the given potential than stars. Therefore, any differences between the cosine and PERLAS potentials might be magnified in gas with respect to the stellar

Table 1. Parameters of the Galactic model.

Parameter	Value	Reference
	Axisymmetric components	
R_0	8.5 kpc	1
Θ_0	220 km s^{-1}	1
Bulge mass	1.41×10^{10} M$_\odot$	1
Disc mass	8.56×10^{10} M$_\odot$	1
Halo mass	8.002×10^{11} M$_\odot$	1
	Spiral arms	
Locus	Logarithmic	2, 3
Arms number	2	4
Pitch angle(i)	15.5 ± 3.5	4
$M_{\rm arms}/M_{\rm disc}$	0.03 ± 0.02	3
Mass	2.7–5.4 $\times 10^9$ M$_\odot$	3
Inner limit	3.3 kpc	ILR position based
Outer limit	12 kpc	CR position based
Scalelength	2.5 kpc	Disc based
Pattern speed ($\Omega_{\rm P}$)	-20 km s^{-1} kpc^{-1}	5

References: (1) Allen & Santillán (1991); (2) Grosbøl & Patsis (1998); (3) Pichardo et al. (2003); (4)Drimmel (2000); (5) Martos et al. (2004).

response. And so, for purposes of comparison, we produce the whole study employing both potentials. In this section, we introduce briefly the cosine and PERLAS potential models and the MHD setup applied to a Milky Way like Galaxy.

In all cases, the spiral arm models are superimposed to the axisymmetric background potential of Allen & Santillán (1991), which includes a Miyamoto–Nagai bulge and disc, and a supermassive spherical halo. Table 1 presents the basic parameters of the axisymmetric background potential.

2.1 Spiral-arm models

2.1.1 Cosine potential

As mentioned before, a large majority of the investigations on the gas associated with spiral-arms model them as a linear perturbation of the axisymmetric background, represented by

$$\Phi_{\rm sp}(R,\phi) = f(R)\,\cos\left[2\phi + g(R)\right], \tag{1}$$

where R, ϕ are cylindrical coordinates, $f(R)$ is the amplitude function of the perturbation, given by Contopoulos & Grosbøl (1986) as $f(R) = -ARe^{\epsilon_{\rm s}R}$, where A is the amplitude and $\epsilon_{\rm s}$ is the inverse of the scalelength. Finally, $g(R)$ describes the geometry of the spiral pattern (*locus*), given by Roberts et al. (1979), as

$$g(R) = -\frac{2}{N\tan i_{\rm p}}\ln[1+(R/R_{\rm s})^N], \tag{2}$$

where $i_{\rm p}$ is the pitch angle, $R_{\rm s}$ is the start position for the spiral arms, and N is a constant that shapes the starting point of the spiral arms, so that $N \to 0$ represents a 180° tip transition from the bar to the spiral arms, while $N \to \infty$ means a 90° tip transition from the bar to the spiral arms. In this work, we set it equal to 100 (for further details; see Pichardo et al. 2003).

2.1.2 PERLAS model

In contrast, the PERLAS spiral arms model (Pichardo et al. 2003) is a bisymmetric, three-dimensional, self-gravitating stationary model based on an adjustable mass distribution, rather than a local arm approximation, as the cosine potential. Several studies have shown that there are differences in the stellar orbital dynamics when the spiral arms are modelled with the cosine potential or with the PERLAS model (Pichardo et al. 2003; Antoja et al. 2009, 2011). Furthermore, chaotic orbital studies have demonstrated that a more detailed spiral arm potential (e.g.the PERLAS model) induces an important fraction of chaos, enough to destroy the spiral structure (Pérez-Villegas et al. 2012, 2013), when all chaotic behaviour was originally attributed to effects produced by the bar, such as overlapping of resonances (Contopoulos 1967; Contopoulos & Harsoula 2012).

PERLAS is constructed by a superposition of individual oblate inhomogeneous spheroids along a given locus (the same than in the cosine potential, equation 2) and superimposed to the axisymmetric background. In this model, the spiral arms have a well-defined mass, unlike the cosine potential, where the spiral arms are treated as a periodic function of the potential not straightforward translatable to mass. The mass assigned to build the spiral arms in the PERLAS model is subtracted from the disc mass. Thus, the inclusion of PERLAS to the Galactic model does not modify the total mass of the original axisymmetric background. In Table 1, we present the parameters of spiral arms that we used in our simulations. For further details about the PERLAS model, we refer the reader to Pichardo et al. (2003).

2.2 Force fitting

In order to compare PERLAS with the cosine potential, we need to fit the spiral arm strength to make them as similar as possible. We achieve this by adjusting the amplitude of the cosine potential (the factor A in equation 1) so that the resulting radial and azimuthal forces approximate the ones obtained using the PERLAS model.

Figs 1 and 2 show the resulting fit for the case of a Milky Way-like galaxy, where the pitch angle is 15.5 and spiral arm mass (in PERLAS) is 3 per cent of the disc mass. In this case, the cosine amplitude A is 650 km^2 s^{-2} kpc^{-1}. In Fig. 1, each panel represents different radial lines, starting in 0° up to 75°. In Fig. 2, each panel shows the computed azimuthal force at different radii, from 4 to 10 kpc. Continuous lines represent PERLAS, dotted lines represent our fit to the cosine potential.

2.3 Spiral arm strength

The spiral strength is related to the pitch angle and the mass of the arm. In the PERLAS model, the spiral arm mass is a small fraction of the disc mass. To quantify the strength of the spiral arms, we calculated the $Q_T(R)$ parameter (Sanders & Tubbs 1980; Combes & Sanders 1981), frequently used to quantify the strength of bars and spiral arms (Buta & Block 2001; Laurikainen & Salo 2002). The value of $Q_T(R)$ is given by

$$Q_T(R) = \frac{F_T^{\rm max}(R)}{|\langle F_R(R)\rangle|}, \tag{3}$$

where $F_T^{\rm max} = |\left(\partial\Phi(R,\theta)/\partial\theta\right)/R|_{\rm max}$ represents the maximum amplitude of the tangential force at radius R, and $\langle F_R(R)\rangle$, is the average axisymmetric radial force. Fig. 3 shows $Q_T(R)$ for the PERLAS (solid line) and cosine (dotted line) potential models, for the case where the spiral arms mass of the PERLAS model has a 3 per cent of the disc mass.

As opposed to Figs 1 and 2, where the force amplitude is almost the same, Fig. 3 shows that there is a difference between both potentials. While the maximum value of Q_T for PERLAS is ∼0.096,

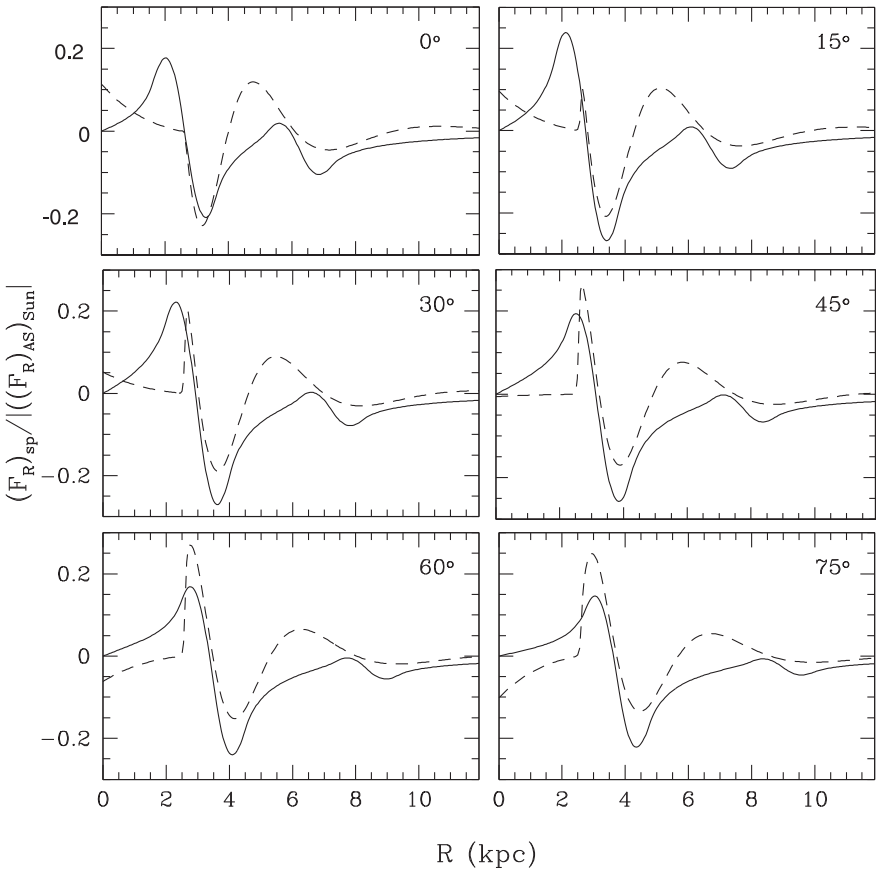

Figure 1. Radial force of the spiral arms along of the different radial lines, starting in 0° up to 165°, each 15°. The radial force is scaled to the axisymmetric background radial force at the solar position. Continuous lines represent PERLAS, dotted lines represent the best fit with equation (1).

for cosine is only ∼0.035. Therefore, if the arm strength is measured using equation (3) instead of the arm force, it is necessary to increase the cosine model amplitude. Fig. 4 shows the Q_T parameter corresponding to an increased cosine amplitude, in this case, $A = 2000\,\mathrm{km^2\,s^{-2}\,kpc^{-1}}$. In this case, since Q_T for the cosine model is larger than PERLAS along all the radial range, this case should be considered as an example to test the gaseous disc response to an extreme cosine model, in order to verify if at this forcing the cosine can reproduce what PERLAS does. In this way, we are bracketing the cosine potential within the values of the force for the PERLAS model.

2.4 The MHD set-up

The initial set-up of the simulations consisted on a gaseous disc, with density profile given by $n(r) = n_0\exp[-(\mathrm{r} - \mathrm{r_0})/\mathrm{r_d}]$, where $n_0 = 1.1\,\mathrm{cm^{-3}}$, $r_0 = 8\,\mathrm{kpc}$ and $r_\mathrm{d} = 15\,\mathrm{kpc}$. The gas follows an isothermal equation of state with temperature $T = 8000\,\mathrm{K}$. Additionally, the gas is permeated by a magnetic field, initially in the azimuthal direction, with an intensity given by $B(r) = B_0\exp[-(r - r_0)/r_B]$, where $B_0 = 5\,\mu\mathrm{G}$ and $r_B = 25\,\mathrm{kpc}$. The disc is set up in rotational equilibrium between the centrifugal force, the thermal and magnetic pressures, magnetic tension and the background axisymmetric potential (Allen & Santillán 1991). This equilibrium is perturbed by the spiral arm potentials under study, both rotating with a pattern speed $\Omega_\mathrm{p} = 20\,\mathrm{kms^{-1}\,kpc^{-1}}$.

We employed the ZEUS code (Stone & Norman 1992a,b) to solve the MHD equations, which is a finite difference, time explicit, operator split, Eulerian code for ideal MHD. We used a 2D grid in cylindrical geometry, with $R \in [1.5, 22]\,\mathrm{kpc}$ and a full circle in the azimuthal coordinate, ϕ, using 750 × 1500 grid points. Both boundary conditions in the radial direction were outflowing. All calculations are performed in the reference frame of the spiral arms. No self-gravity of the gas was considered.

3 RESULTS

We present in this section a comparison between the gas response to the simplified cosine potential for the spiral arms, and the density distribution based model PERLAS. In the limit for weak and/or small pitch angles (approximately linear regime), both models behave very similar as expected, however, for stronger arms (more massive or larger pitch angles), from this comparison we find severe differences in the gas behaviour and formation of spiral arms and branch-like structures. The deviation of the response between both models is induced by the basic differences of these potentials. We then present an interpretation on the presence of galactic branches prior to the ultraharmonic 4:1 resonance and connect them to a possible signature of transient spiral arms.

3.1 Gas response comparison: PERLAS *versus* cosine potential models

In order to compare both potentials, we fit the cosine potential with PERLAS to make it as similar as possible in the force amplitude (Section 2.2). In all cases, the axisymmetric gaseous disc, initially in

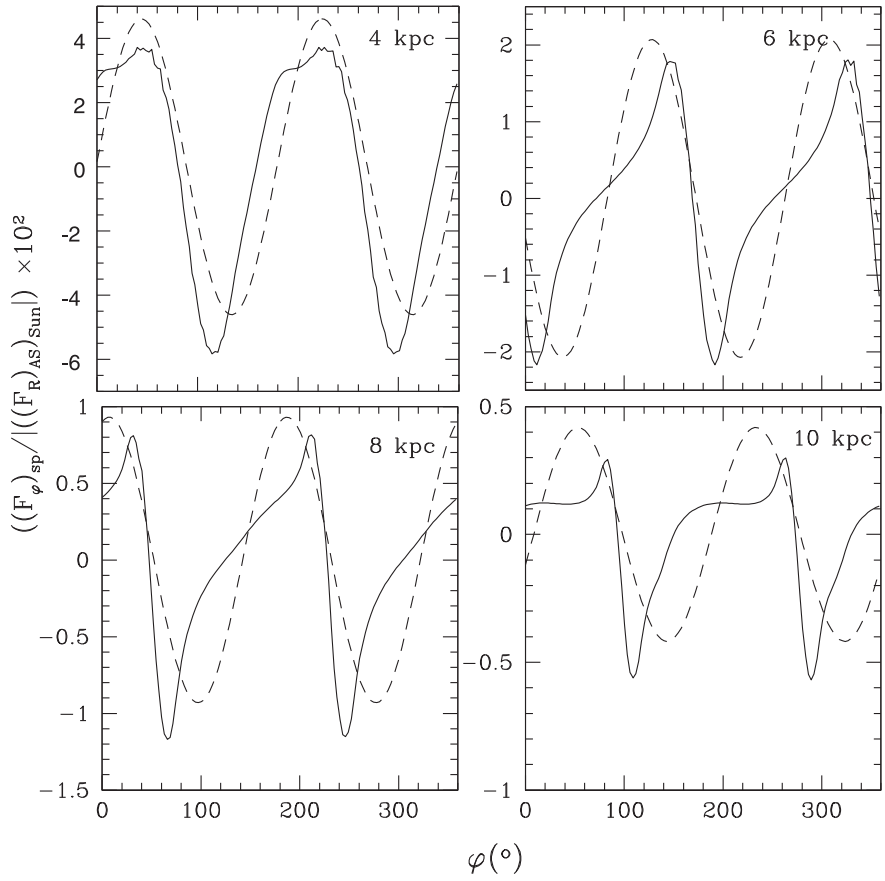

Figure 2. Azimuthal force at the different radius, from 4 to 10 kpc, each 2 kpc. The radial force is scaled to the axisymmetric background radial force at the solar position. Continuous lines represent PERLAS, dotted lines represent our fit with equation (1).

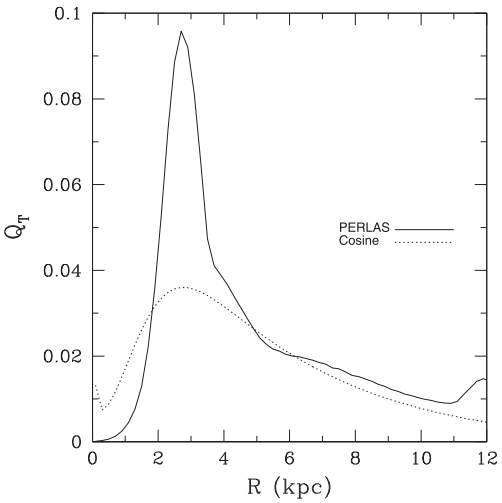

Figure 3. $Q_T(R)$ parameter for the spiral arms of a Milky Way-like galaxy for the PERLAS (solid line) and cosine (dotted line) potential models.

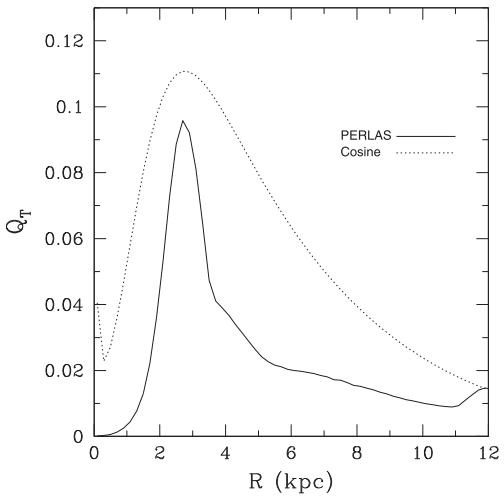

Figure 4. Similar to Fig. 3, with the amplitude of the cosine model increased.

rotational equilibrium, was perturbed by the spiral potential either PERLAS or the cosine.

As mentioned already, the cosine potential represents a simple solution from the density wave linear theory, self-consistent for tightly wound spiral arms (TWA, i.e. where the perturbation is very small, which means small pitch angles or with very reduced masses). The Milky Way Galaxy and the most of spiral galaxies are actually far from this regime. Thus, it should not be surprising that the gaseous disc (Gómez et al. 2013) and the stellar orbits (Pérez-Villegas et al. 2012) show a different structure when subjected to a self-gravitating, more realistic model instead of a local approximation. With this in mind, the gaseous disc response to both models should be similar if we focus on a region of the parameter space where both potentials are valid, i.e. if we set PERLAS and the cosine potential so that it is approximately in the linear regime, with a very small pitch angle

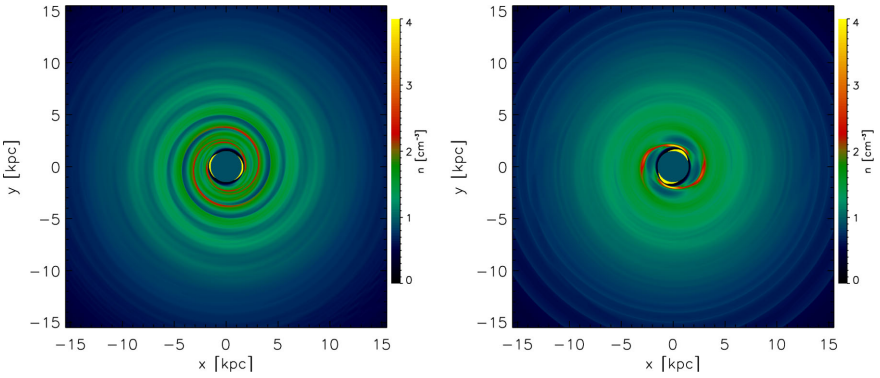

Figure 5. Density distribution for the simulation with the cosine potential (left-hand panel) and with the PERLAS model in the linear regime (right-hand panel) after 1.2 Gyr. In both cases, the pitch angle is 6°. The amplitude for the cosine potential is $A = 100\,\mathrm{km^2\,s^{-2}\,kpc^{-1}}$ and the spiral arm mass for the PERLAS model is 1 per cent of the stellar disc mass.

and spiral arm mass. In Fig. 5, we show the linear regime for both potentials. The density distribution with the cosine potential is presented in the left-hand panel and PERLAS model in the right-hand panel, the pitch angle is 6°, the spiral arms mass is 1 per cent of the disc mass, $A = 100\,\mathrm{km^2\,s^{-2}\,kpc^{-1}}$. Indeed, the gas response to the potentials is similar as expected, forming two spiral arms in both cases.

For the specific case of a Milky Way-like galaxy, we constructed a model that reproduces some of the observational parameters for the background and spiral arms potential to compare them with the cosine potential for the spiral arms (force fitted with PERLAS). The spiral arms pattern angular speed is $20\,\mathrm{km\,s^{-1}\,kpc^{-1}}$, on a logarithmic locus with a pitch angle of 15.°5. The mass of spiral arm for PERLAS model is 3 per cent of the disc mass, which is equivalent to a cosine amplitude of $A = 650\,\mathrm{km^2\,s^{-2}\,kpc^{-1}}$, when the non-axisymmetric force is employed for the fitting (see Section 2.2), and $A = 2000\,\mathrm{km^2\,s^{-2}\,kpc^{-1}}$, when the arm strength (i.e. the Q_T parameter) is considered for the fitting instead (see Section 2.3). We follow the evolution of the system for 5 Gyr.

Fig. 6 shows the resulting density distribution of the gaseous disc when is perturbed by the cosine potential with a small amplitude ($A = 650\,\mathrm{km^2\,s^{-2}\,kpc^{-1}}$). After the simulation starts, the gas very rapidly settles into a spiral pattern, forming two spiral arms at 30 Myr (top-left panel). 300 Myr into the simulation (top-right panel), the two spiral arms are better defined, and the gas is forming a secondary structure. As simulation progresses (1.5 and 3 Gyr, bottom panels), the gas continues responding to the spiral arms and even more substructure forms, but the large-scale density response consists of two arms only. The pitch angle of the formed arms is ∼15.°5, equal to the imposed potential at the beginning of the simulation. In the last panel, a gas instability at the corotation radius is seen, as reported previously (Martos et al. 2004; Gómez et al. 2013).

In contrast, Fig. 7 shows the density distribution of the gaseous disc when is perturbed by the PERLAS spiral arm potential. The gas very rapidly settles into a spiral pattern, as in the cosine potential case, forming two spiral arms at 30 Myr. At 300 Myr and later, the gas forms four spiral arms instead of the two arms in the cosine potential simulation. Even though the simulation develops four spiral arms, these are associated in two pairs, each composed of a strong arm and a weak arm. The strong arms have a pitch angle of ∼15°, and the weak arms have a pitch angle of ∼7°. This doubling of the spiral arms in the gas response has been seen in other MHD simulations using the PERLAS model (Martos et al. 2004; Gómez et al. 2013, see also Section 3.2).

In Section 2.3, we noted that the spiral arm strength, as measured by equation (3), was very different for both potentials, even if the force amplitudes were almost the same. Therefore, we decided to perform a second experiment with a larger amplitude $A = 2000\,\mathrm{km^2\,s^{-2}\,kpc^{-1}}$ for the cosine potential, that would be equivalent to a factor of ∼3 times the force of PERLAS. This much larger amplitude for the cosine potential is stronger than PERLAS at any radii, as shown in Fig. 4. The purpose of this overestimated experiment was to test if the four spiral arms formed with PERLAS were due to the strength of spiral arms only. Fig. 8 shows the gas density distribution resulting from perturbing the disc with the larger force amplitude of the cosine potential. It is readily seen that the effect of the spiral potential on the gas disc is larger and generates more substructure, but the gas still responds forming two spiral arms, unlike the density based potential PERLAS that forms four arms for larger pitch angles, i.e. for stronger arms. Consequently, this difference does not come from the force amplitude, but it seems rather originated from the self-gravitating nature and specific details of the potential that a local approximation for the forces given by the cosine potential is unable to reproduce. We further explain this in the next section.

3.2 Branch formation and their relation with the transient nature of spiral arms

In Section 3.1, we showed that the intrinsic differences in the nature of the cosine and PERLAS potentials induce a distinct gaseous arm structure as compared to a disc perturbed by a cosine arm potential. While employing the spiral arm cosine potential, a bisymmetric gaseous structure seems to be an invariable outcome, for the PERLAS potential a two- or four-armed structure could be obtained. This result points to the necessity of understanding how the gas responds to the PERLAS model when we vary the structural parameters of the spiral arms, such as its mass and pitch angle, considering the uncertainties in the determination of these parameters for the Milky Way's spiral arms. Therefore, we developed a set of simulations varying spiral arm pitch angles (i) and spiral arms masses. We present here some of them ranging from 12° to 19°, and the mass of the spiral arms (M_{sp}), from 1.75 per cent to 5 per cent of the total disc mass (M_{D}).

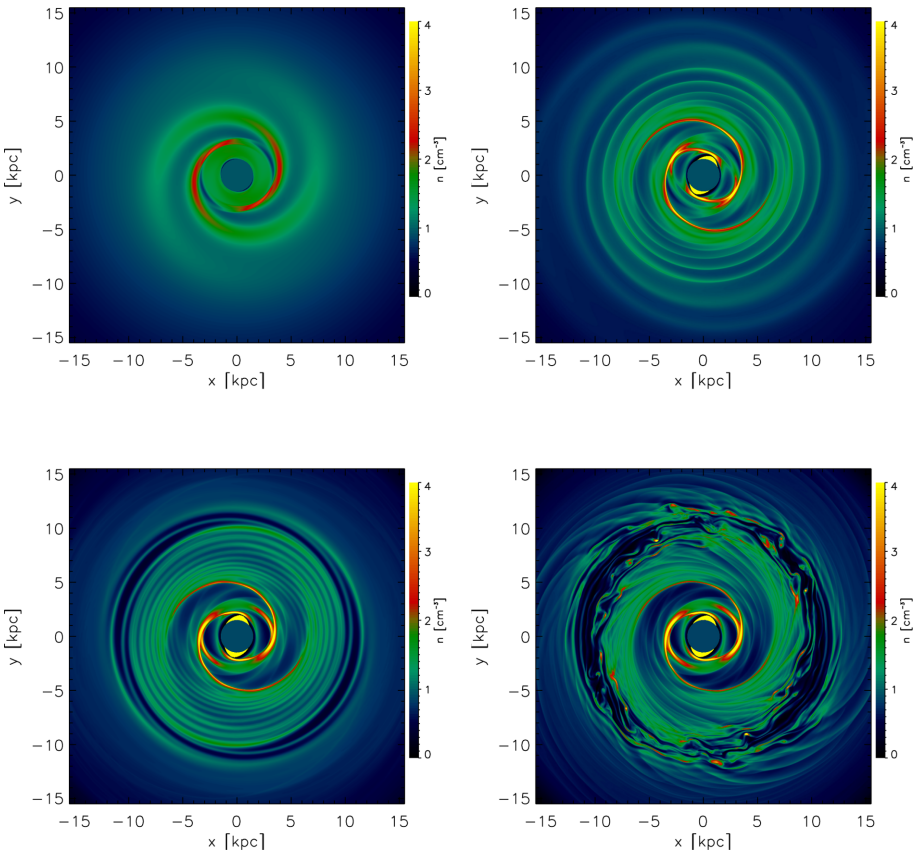

Figure 6. Density distribution using a cosine potential to model spiral arms. Times shown in this plot correspond to 30 Myr after the simulation starts (top-left panel), 300 Myr (top-right panel), 1.5 Gyr (bottom left), and 3 Gyr (bottom right).

Fig. 9 shows a mosaic of simulations. The panels in the left-hand column are the stable periodic stellar orbits and the panels in the right-hand column are the gas density distribution after 1.2 Gyr. The maximum density response (where the orbits crowd producing a density enhancement) quantifies the orbital support to a given spiral perturbation through periodic orbits. We computed the stellar periodic orbits in order to explore the orbital support to the imposed PERLAS spiral arm potential (open squares in the left-hand panels of Fig. 9). To estimate the density response, we employ the method of Contopoulos & Grosbøl (1986). This method assumes that stars in circular orbits in an axisymmetric potential, with the same sense of rotation of the spiral arms, are trapped around the corresponding periodic orbit in the presence of the spiral arms. For this purpose, we calculated a set of central periodic orbits (between 50 and 60) and found the density response along them using the conservation of the mass flux between any two successive periodic orbits. With this information we seek the position of the maximum density response along each periodic orbit (filled squares in the left-hand panels of Fig. 9). These positions are compared with the imposed spiral arms (PERLAS model). The method implicitly considers a small dispersion (with respect to the central periodic orbit) since it studies a region where the flux is conserved. On the other hand, this dispersion is based on parameters for the galaxies where dynamics is quite ordered, orbits follow their periodic orbit closely, in such a way that we consider this study a good approximation. This method to estimate the density response has been widely used in literature (Contopoulos & Grosbøl 1988; Amaral & Lepine 1997; Pichardo et al. 2003; Yano, Kan-Ya & Gouda 2003; Voglis, Stavropoulos & Kalapotharakos 2006; Tsoutsis, Efthymiopoulos & Voglis 2008; Pérez-Villegas et al. 2012, 2013; Junqueira et al. 2013). We refer the reader to the work of Contopoulos & Grosbøl (1986) for more details. With this in mind, a model in Fig. 9 where the open and filled squares coincide would represent a stable, approximately orbitally self-consistent system, while a lack of coincidence would mean that the spiral is unlikely to be long lasting (Pérez-Villegas et al. 2012, 2013).

For $M_{sp} = 0.0175 M_D$ and $i = 12^\circ$ (upper-left panel of Fig. 9), the stellar density response follows approximately the imposed spiral potential prior to the 4/1 resonance. After that, the stellar response forms a slightly smaller pitch angle than the imposed spiral. In the MHD simulation, the gaseous disc responds to the two-arm potential with the now familiar four spiral-armed structure, where the pitch angle of the stronger pair of arms corresponds to that of the imposed pitch angle potential, while the other pair of gaseous arms has a systematically smaller pitch angle, corresponding closely to the regions of periodic orbits crowding. Now, with the same spiral arm mass but a pitch angle of $i = 19^\circ$ (second row of Fig. 9), the stellar density response (i.e. periodic orbits) forms again a smaller pitch angle compared with the imposed, while in the gas, the four spiral arms seem stronger and the difference in the pitch angle between the gaseous and imposed arms is larger than the previous case. For $M_{sp} = 0.05 M_D$ and $i = 12^\circ$ (third row), the stellar density response closely follows the imposed spiral arm potential prior to the 4/1 resonance. After that, the stellar response forms a slightly smaller pitch angle than the imposed spiral, while the gas responds with four spiral arms, but the second pair is very weak but with a significantly smaller pitch angle than the imposed spiral arm potential. Finally, with the same spiral arm mass (5 per cent of the disc mass) but a pitch

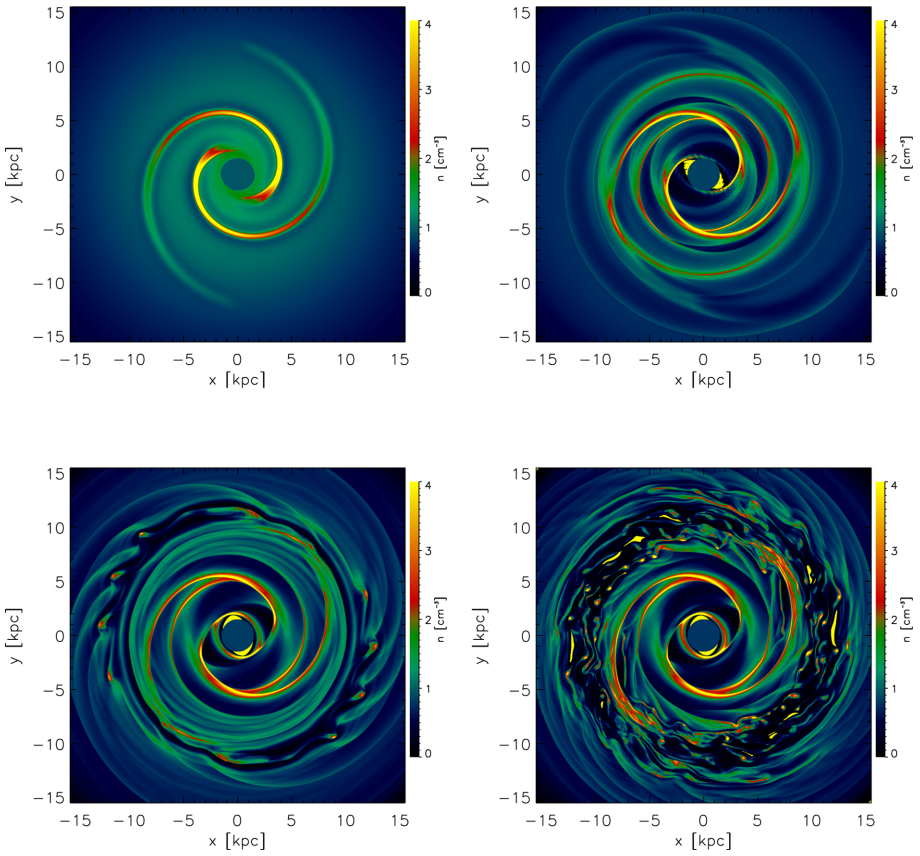

Figure 7. Density distribution using the PERLAS spiral arm model. Panels correspond to the same evolution times as in Fig. 6

angle of $i = 19^\circ$ (fourth row), we found no periodic orbits beyond 4/1 resonance and the stellar density response forms a pitch angle smaller than 19°. The gaseous disc responds with well-defined four spiral arms that extend up to the corotation radius. Note that in this last simulation, there is not much that can be said about the (stellar or gaseous) orbital support since periodic orbits tend to disappear due to the strong forcing of the imposed spiral arms, meaning that spiral arms would rather be transient by construction in this case and the MHD gaseous disc behaviour is difficult to predict from periodic orbit computations. However, such as the stellar arms constructed in this case, the gaseous spiral would be transient in likely even shorter time-scales than in the case where periodic orbits exist but settle down systematically in smaller pitch angles than the original imposed spiral arms in the region where periodic orbits do exist. Note that, in general, the arms that should eventually disappear in this scenario, are the stronger stellar imposed spiral arms (see second row of Fig. 9; Pérez-Villegas et al. 2013).

Therefore, the stellar response density maxima represent the regions of the arms where stars would crowd for long time-scales, this is, where the existence of stable, long-lasting spiral arms would be more likely. On the other hand, if the stellar density response forms a spiral arm with a different pitch than the imposed angle, then the imposed spiral arms triggered on the disc (by a bar, an interaction, etc.), would rather be structures of transient nature since those are not orbitally supported (Pérez-Villegas et al. 2013). Likewise, for the case of the spiral arms in the Milky Way, the values frequently seen in literature for the pitch angle, range from ∼11° to 19°. These values and the knowledge of the galactic type could provide some information about their nature, i.e. whether they are long-lasting or transient structures. Following the pitch angle restrictions found by Pérez-Villegas et al. (2013), the larger pitch angle values reported in the literature for the Milky Way galaxy would imply that its spiral arms are a transient feature. The formation of four spiral arms in the gas response is, in this scenario, another piece of evidence of a transient nature of the spiral arms in the Milky Way galaxy, as we claim it is the secondary pair of arms in Fig. 9, that coincides more closely with the stellar density response from periodic orbits, as expected from Gómez et al. (2013). Summarizing, the first (imposed) pair of massive spiral arms formed in the disc, with a larger pitch angle, triggers a second pair of arms (traced approximately by the periodic orbits), with smaller pitch angles (Pérez-Villegas et al. 2013). In this outline, the gas responds forming a second pair of arms aligned with the locus of the orbital crowding. This lighter structures would likely be preferentially formed by young stars and gas than by evolved stars because of their transient nature, i.e. similar to what we call 'branches'. Finally, in this framework, the presence of clear and strong branches in spiral galaxies, with smaller pitch angles than the corresponding couple of massive spiral arms on a galaxy, would be a signature of the transient nature of the spiral arms in a given galaxy. On the other hand, spiral galaxies without evidence of branches could indicate the presence of a longer lasting spiral arm structure.

4 DISCUSSION AND CONCLUSIONS

With the use of a detailed three-dimensional, density-distribution based potential for the spiral arms, combined with MHD simulations on a Milky Way-like galactic disc, we have studied the stellar orbital and gaseous response to the galactic potential. As a first experiment, we constructed a simple cosine potential (as the ones commonly

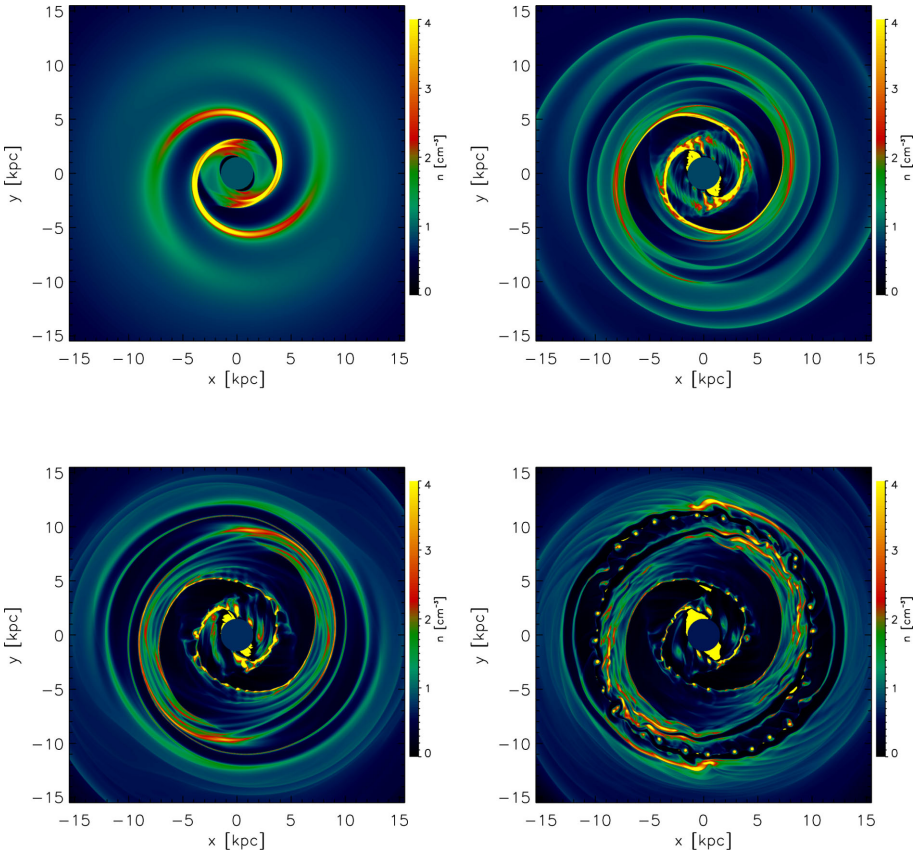

Figure 8. Gas density distribution for the simulation with the cosine potential when its force amplitude is increased by a factor of ∼3 (up to the value provided by PERLAS model). The times shown correspond to 30 Myr (top-left panel), 300 Myr (top-right panel), 900 Myr (bottom-left panel), and 1.5 Gyr (bottom-right panel).

employed in literature) that reproduced approximately what the density based potential PERLAS exerts on the stellar and gaseous dynamics.

The first set of simulations compare the gas response when the disc is perturbed by both spiral arm potential models. We also varied the structural parameters of the spiral arms in the PERLAS model, such as the pitch angle (12°–19°) and the mass of spiral arms (1.75 per cent to 5 per cent of the stellar disc mass) in order to understand how these parameters affect the gaseous disc dynamics. Additionally, we constructed stellar periodic orbits and calculate the stellar response density maxima.

With these exercises, we found that only in the case of the PERLAS model the gas and stellar density response (based on the existence of periodic orbits) is a consistent four-armed spiral structure: a couple of strong gaseous arms located at the position of the imposed stellar arms, and a second pair of weaker gaseous arms located at the position of the stellar orbit crowding. Since the potential and the stellar density response do not coincide, the spiral arms are prone to destruction. So, the presence of the second (gaseous) pair is interpreted as a sign of this transiency.

Our main conclusions can be summarized as follows.

(i) We performed a study of the gas response to two galactic potentials: the density distribution based model PERLAS and the widely employed in the literature cosine potential. We verified that the gas response (a two-armed structure) is the same for both models close to the linear regime only, i.e. for low-mass spiral arms and pitch angles smaller than ∼10°. In the general case, however (i.e. large pitch angle or arm mass), even when the cosine potential has been fitted as close as possible to the PERLAS model, they produce quite distinct outcomes on the gas response. In the case of the cosine potential, the gas responds invariably forming two spiral arms while, with the PERLAS model, the gas responds with four gaseous spiral arms (in the general strong arm case).

(ii) We increased the strength of the spiral arms represented by the cosine potential up to a point the arms were equivalent and even beyond the mass of a strong bar as an experiment to try to reproduce the gas response provided by the PERLAS model. However, the answer was always a bisymmetric structure. We conclude that the spiral arm strength is not responsible for the four-arm gas response, but rather it is the product of the forcing generated by the whole density distribution better represented by the PERLAS model that, in turn, forces the periodic orbit response to shift its crowding regions inside the imposed locus of the massive spiral arms.

(iii) Using the PERLAS model, we changed the structural parameters of the spiral arms according to the observational and theoretical uncertainties in the determination of the Milky Way's spiral arms in the literature. Within these values, for the general case, the stellar response density maxima systematically forms spiral arms with a smaller pitch angle than the imposed spiral, meaning that the spiral arms might be a transient feature in the Milky Way Galaxy (Pérez-Villegas et al. 2013). The presence of a second pair of lighter spiral arms ('branches'), with smaller pitch angles induced by the first more massive stellar spiral arms, might be evidence of the lack of support to the stronger arms on a galactic disc, and therefore evidence of the transient nature of spiral arms in a given galaxy.

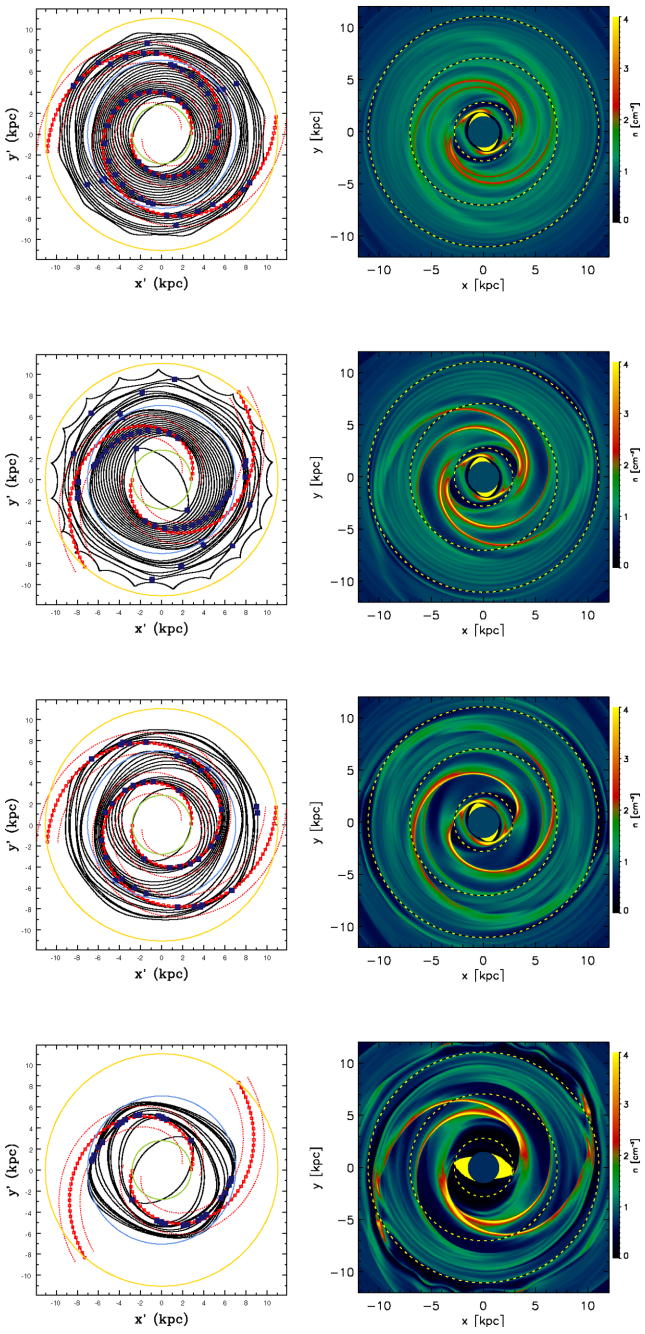

Figure 9. Stellar and gaseous response to different parameters of the spiral arm model (PERLAS). Panels on the left-hand column show the stable periodic stellar orbits (black solid lines), the response density maxima (filled squares), and the imposed spiral arm locus (open squares), flanked by two dotted lines that represent the spiral arm width. Coloured circles represent the position of the inner Lindblad (green), 4/1 (blue) and corotation (yellow) resonances. Panels on the right-hand column show the gas density distribution after 1.2 Gyr, together with the inner Lindblad, 4/1 and corotation resonances (dashed circles). The mass of spiral arms and pitch angle are: $M_{\rm sp} = 0.0175 M_{\rm D}$ with $i = 12^{\circ}$ (first row) and $i = 19^{\circ}$ (second row), $M_{\rm sp} = 0.05 M_{\rm D}$ with $i = 12^{\circ}$ (third row) and $i = 19^{\circ}$ (fourth row).

Applying this scenario to the Milky Way, for the stronger spiral arm values reported in literature (i.e. pitch angles larger than $\sim 10^{\circ}$, and masses larger than ~ 2 per cent of the disc), the spiral arms in the Milky Way would be of transient nature.

(iv) Although in this work we applied the models to Milky Way-like galactic discs, it is worth noticing that the results are general. This means that the presence of branches with smaller pitch angles than the main arms might be the 'smoking gun' that proves transiency of spiral arms in any given galaxy.

ACKNOWLEDGEMENTS

We thank Edmundo Moreno for enlightening discussions that helped to improve this work. APV acknowledges the support of the postdoctoral Fellowship of DGAPA-UNAM, México. This work has received financial support from DGAPA PAPIIT grants IN111313 and IN114114.

REFERENCES

Allen C., Santillán A., 1991, Rev. Mex. Astron. Astrofis., 22, 256
Amaral L. H., Lepine J. R. D., 1997, MNRAS, 286, 885
Antoja T., Valenzuela O., Pichardo B., Moreno E., Figueras F., Fernández D., 2009, ApJ, 700, L78
Antoja T., Figueras F., Torra J., Valenzuela O., Pichardo B., 2010, in Ulla A., Manteiga M., eds, Lecture Notes and Essays in Astrophysics, Vol. 4, The Origin of Stellar Moving Groups. Trculo Press, Vigo, Spain, p. 13
Antoja T., Romero-Gómez M., Figueras F., Valenzuela O., Pichardo B., Moreno E., 2011, MNRAS, 418, 1423
Artymowicz P., Lubow S. H., 1992, ApJ, 389, 129
Balbus S. A., 1988, ApJ, 324, 60
Barbanis B., Woltjer L., 1967, ApJ, 150, 461
Benjamin R. A. et al., 2005, ApJ, 630, L149
Buta R., Block D. L., 2001, ApJ, 550, 243
Chakrabarti S., Laughlin G., Shu F. H., 2003, ApJ, 596, 220
Combes F., Sanders R. H., 1981, A&A, 96, 164
Contopoulos G., 1967, Bull. Astron. (Ser. 3), 2, 223
Contopoulos G., Grosbøl P., 1986, A&A, 155, 11
Contopoulos G., Grosbøl, 1988, A&A, 197, 83
Contopoulos G., Harsoula M., 2012, Celest. Mech. Dyn. Astron., 113, 81
Corder S., Sheth K., Scoville N. Z., Koda J., Vogel S. N., Ostriker E., 2008, ApJ, 689, 148
D'Onghia E., Vogelsberger M., Hernquist L., 2013, ApJ, 766, 34
Dobbs C. L., Bonnell I. A., 2006, MNRAS, 367, 873
Dobbs C. L., Burkert A., Pringle J. E., 2011, MNRAS, 417, 1318
Donner K. J., Thomasson M., 1994, A&A, 290, 785
Drimmel R., 2000, A&A, 358, L13
Drimmel R., Spergel D. N., 2001, ApJ, 556, 181
Dwek E. et al., 1995, ApJ, 445, 716
Eden D. J., Moore T. J. T., Morgan L. K., Thompson M. A., Urquhart J. S., 2013, MNRAS, 431, 1587
Elmegreen D. M., 1980, ApJ, 242, 528
Englmaier P., Gerhard O., 1999, MNRAS, 304, 512
Feitzinger J. V., Schwerdtfeger H., 1982, A&A, 116, 117
Foyle K., Rix H.-W., Walter F., Leroy A. K., 2010, ApJ, 725, 534
Foyle K., Rix H.-W., Dobbs C. L., Leroy A. K., Walter F., 2011, ApJ, 735, 101
Fujimoto M., 1968, in Arakelyan A., ed., Proc. IAU Symp. 29, Non-stable Phenomena in Galaxies. Armenian Academy of Science, Armenia, p. 453
Fux R., 1999, A&A, 345, 787
Gómez G. C., Pichardo B., Martos M. A., 2013, MNRAS, 430, 3010
Grosbøl P. J., Patsis P. A., 1998, A&A, 336, 840
Junqueira T. C., Lépine J. R. D., Braga C. A. S., Barros D. A., 2013, A&A, 550, AA91
Kawata D., Hunt J. A. S., Grand R. J. J., Pasetto S., Cropper M., 2014, MNRAS, 443, 2757
Kim Y., Kim W.-T., 2014, MNRAS, 440, 208
Kim W.-T., Ostriker E. C., 2002, ApJ, 570, 132

Kim W.-T., Ostriker E. C., 2006, ApJ, 646, 213
Kim W.-T., Kim Y., Kim J.-G., 2014, ApJ, 789, 68
Laurikainen E., Salo H., 2002, MNRAS, 337, 1118
Lee W.-K., Shu F. H., 2012, ApJ, 756, 45
Lin C. C., Shu F. H., 1964, ApJ, 140, 646
Lynds B. T., 1970, in Becker W., Contopoulos G., eds, Proc. IAU Symp. 38, The Spiral Structure of our Galaxy. Reidel, Dordrecht, p. 26
Martínez-García E. E., González-López lira R. A., 2013, ApJ, 765, 105
Martos M., Hernandez X., Yáñez M., Moreno E., Pichardo B., 2004, MNRAS, 350, L47
Matsumoto T., Hayakawa S., Koizumi H., Murakami H., Uyama K., Yamagami T., Thomas J. A., 1982, in Riegler G. R., Blandfordeds R. D., AIP Conf. Proc. Vol. 83, The Galactic Center. Am. Inst. Phys., New York, p. 48
Moore T. J. T., Urquhart J. S., Morgan L. K., Thompson M. A., 2012, MNRAS, 426, 701
Patsis P. A., Hiotelis N., Contopoulos G., Grosbol P., 1994, A&A, 286, 46
Patsis P. A., Grosbol P., Hiotelis N., 1997, A&A, 323, 762
Pérez-Villegas A., Pichardo B., Moreno E., Peimbert A., Velázquez H. M., 2012, ApJ, 745, L14
Pérez-Villegas A., Pichardo B., Moreno E., 2013, ApJ, 772, 91
Pichardo B., Martos M., Moreno E., Espresate J., 2003, ApJ, 582, 230
Roberts W. W., 1969, ApJ, 158, 123
Roberts W. W., Jr, Huntley J. M., van Albada G. D., 1979, ApJ, 233, 67
Roca-Fàbrega S., Valenzuela O., Figueras F., Romero-Gómez M., Velázquez H., Antoja T., Pichardo B., 2013, MNRAS, 432, 2878
Roca-Fàbrega S., Antoja T., Figueras F., Valenzuela O., Romero-Gómez M., Pichardo B., 2014, MNRAS, 440, 1950
Roškar R., Debattista V. P., Quinn T. R., Wadsley J., 2012, MNRAS, 426, 2089
Sanders R. H., Tubbs A., 1980, AJ, 235, 803
Scarano S., Lépine J. R. D., 2013, MNRAS, 428, 625
Scoville N. Z., Polletta M., Ewald S., Stolovy S. R., Thompson R., Rieke M., 2001, AJ, 122, 3017
Sellwood J. A., 2011, MNRAS, 410, 1637
Sellwood J. A., Carlberg R. G., 2014, ApJ, 785, 137
Seo W.-Y., Kim W.-T., 2014, ApJ, 792, 47
Shetty R., Ostriker E. C., 2006, ApJ, 647, 997
Shu F. H., Milione V., Roberts W. W., Jr, 1973, ApJ, 183, 819
Sofue Y., 1976, A&A, 48, 1
Stone J. M., Norman M. L., 1992a, ApJS, 80, 753
Stone J. M., Norman M. L., 1992b, ApJS, 80, 791
Tsoutsis P., Efthymiopoulos C., Voglis N., 2008, MNRAS, 387, 1264
Vallée J. P., 2002, ApJ, 566, 261
Vallée J. P., 2013, Int. J. Astron. Astrophys., 3, 20
Voglis N., Stavropoulos I., Kalapotharakos C., 2006, MNRAS, 372, 901
Wada K., Koda J., 2004, MNRAS, 349, 270
Wada K., Baba J., Saitoh T. R., 2011, ApJ, 735, 1
Weaver H. F., 1970, in Habing H. J., ed., Proc. IAU Symp. 39, Interstellar Gas Dynamics. Reidel, Dordrecht, p. 22
Weiner B. J., Sellwood J. A., 1999, ApJ, 524, 112
Yañez M. A., Norman M. I., Martos M. A., Hayes J. C., 2008, ApJ, 672, 207
Yano T., Kan-Ya Y., Gouda N., 2003, PASJ, 55, 409
Zhang X., 1998, ApJ, 499, 93
Zhao H., 1996, MNRAS, 283, 149

This paper has been typeset from a TEX/LATEX file prepared by the author.